This is an open access article published under an ACS AuthorChoice License, which permits copying and redistribution of the article or any adaptations for non-commercial purposes.

molecular pharmaceutics

Article

pubs.acs.org/molecularpharmaceutics

Preloading with Unlabeled CA19.9 Targeted Human Monoclonal Antibody Leads to Improved PET Imaging with ^{89}Zr-5B1

Jacob L. Houghton,[†,&] Dalya Abdel-Atti,[†] Wolfgang W. Scholz,[‡] and Jason S. Lewis*[,†,§]

[†]Department of Radiology, Memorial Sloan Kettering Cancer Center, New York, New York 10065, United States

[‡]MabVax Therapeutics, San Diego, California 92121, United States

[§]Molecular Pharmacology Program, Memorial Sloan Kettering Cancer Center, New York, New York 10065, United States

Supporting Information

ABSTRACT: CA19.9 is one of the most commonly occurring and highest density antigens in >90% of pancreatic cancers, making it an excellent target for monoclonal antibody (mAb)-based imaging and therapy applications. Preloading of unlabeled antibodies to enhance targeting of a radiolabeled mAb has been previously described both for imaging and radioimmunotherapy studies for other targets. We investigated the effect of preloading with the unmodified anti-CA19.9 antibody 5B1 on the uptake and contrast of the PET tracer ^{89}Zr-5B1 in subcutaneous and orthotopic murine models of pancreatic cancer utilizing Capan-2 xenografts, known to both express CA19.9 and shed antigen into circulation. Biodistribution and PET imaging studies with ^{89}Zr-5B1 alone showed high levels in the liver, spleen, and lymph nodes of mice with subcutaneous Capan-2 tumor xenografts when administered without preinjection of 5B1. When unlabeled 5B1 was administered prior to ^{89}Zr-5B1, the tracer significantly enhanced image contrast and tumor to tissue ratios in the same model, and the improvement was related to the time interval between the injections. Moreover, tumors were clearly delineated in an orthotopic pancreatic cancer model using our optimized approach. Taken together, these data suggest that preloading with 5B1 can improve ^{89}Zr-5B1 imaging of disease in a Capan-2 mouse model and that exploration of preloading may have clinical utility for ongoing clinical investigations.

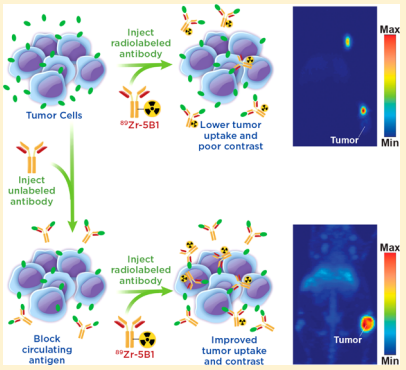

KEYWORDS: *pancreatic cancer, PET imaging, CA19.9, 5B1*

INTRODUCTION

Pancreatic cancer remains one of most deadly forms of cancer. In the United States, it currently accounts for 3% of new cancer cases and 7% of cancer deaths, and is projected to be the second leading cause of cancer deaths by 2030.[1,2] Frontline therapies remain inadequate, and recent advances have only marginally improved outcomes for patients. There is a pressing need for new therapeutic strategies in the fight against pancreatic cancer, and a wide range of clinical trials are currently aiming to make inroads against the disease.[3]

Therapies based on monoclonal antibodies (mAb) are one promising option for molecularly targeted therapy of pancreatic cancer. The appeal is primarily due to the high affinity and specificity they may show for their target antigens. In addition to their potential as stand-alone immunotherapeutics, mAbs may also serve as a platform for delivering cytotoxic chemotherapies (antibody−drug conjugate; ADC) or therapeutic radioisotopes (radioimmunotherapy; RIT).

CA19.9 is one of the most widely studied and oft employed serum biomarkers for pancreatic cancer, providing information regarding therapeutic response, overall survival, and the likelihood of recurrence in patients with established disease.[4] However, the utility of serum CA19.9 levels as a management or diagnostic tool in pancreatic cancer is moderated by the fact that increased expression is also observed in a number of benign conditions and unrelated malignancies. Nonetheless, CA19.9 remains an attractive target for molecularly targeted therapeutics and diagnostics because it is the most common biomarker in pancreatic cancer and is preferentially expressed on the surface of cancer cells at extremely high concentrations.

For these reasons, a number of antibody-based agents targeting CA19.9 have been developed in the past decade.[5−7] One of the most promising agents is 5B1, which is a fully human, anti-CA19.9 mAb that is currently being investigated as both a stand-alone immunotherapeutic and a PET imaging agent for CA19.9-positive malignancies in preclinical models of cancer, including pancreatic cancer.[8−11] However, imaging with an anti-CA19.9 directed mAb may be complicated by the fact that CA19.9 is also shed from the tumor into circulation. Circulating CA19.9 may create a pool of antigen that binds to the tracer mAb limiting its ability to bind to the target tissue. Antigen expression in nontumor tissue, including the blood, has been problematic for other ^{89}Zr-labeled mAbs.[12,13] In radio-

Received: December 16, 2016
Revised: February 3, 2017
Accepted: February 13, 2017
Published: February 13, 2017

 © 2017 American Chemical Society

DOI: 10.1021/acs.molpharmaceut.6b01130
Mol. Pharmaceutics 2017, 14, 908−915

logical applications, the binding of radiolabeled mAb to circulating CA19.9 may also increase residence time in the blood, reducing tumor to tissue contrast and increasing the dosimetric burden in imaging or RIT applications.[9,10]

Circulating tumor antigens have been an obstacle in numerous clinical trials with ^{89}Zr-labeled antibodies, including both ^{89}Zr-rituxumab and ^{89}Zr-trastuzumab.[12−14] However, effective strategies for overcoming antigen sinks to provide images with enhanced contrast at target tissues have been developed. In the case of ^{89}Zr-rituxumab, preloading with unlabeled rituximab prior to injection reduced uptake of the radiotracer in the spleen and circulating B cells, leading to improved image quality in patients with circulating CD20+ lymphocytes.[12] Similarly, it was shown that injection of a large dose of unmodified trastuzumab immediately before ^{89}Zr-trastuzumab, which in essence served to lower the specific activity at the time of injection, also led to improved image quality dependent upon total tumor burden of the patient.[13] These "preloading" strategies offer a means to improve delivery of a targeted antibody agent to the tissue of interest (Figure 1).

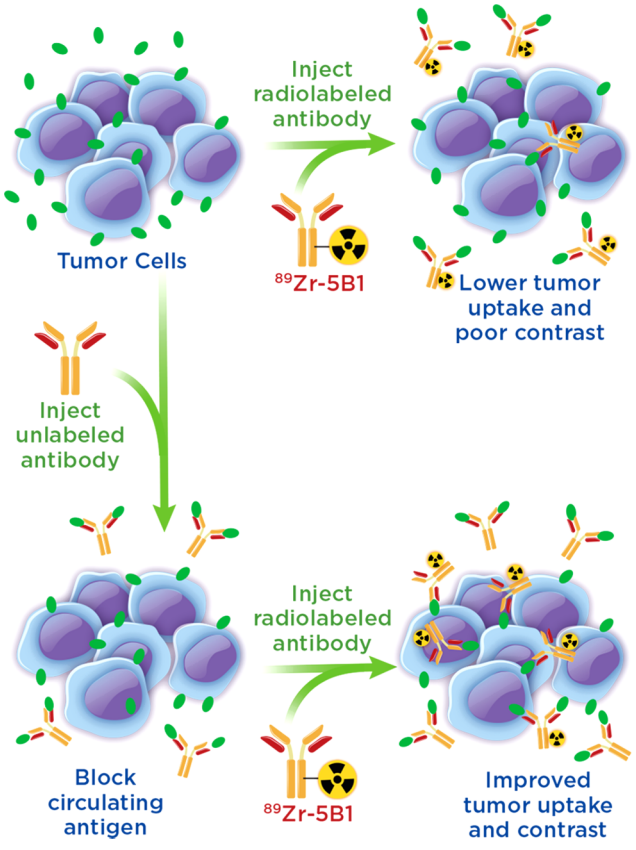

Figure 1. Illustration of the benefits of a preloading strategy in which unlabeled antibody is injected to bind circulating antigen prior to injection of the radiolabeled antibody allowing for decreased sequestration in the blood and increased uptake of the radiotracer.

We modeled the presence of a serum CA19.9 antigen sink in subcutaneous and orthotopic murine models of pancreatic cancer using the Capan-2 cell line, which is known to both express and shed CA19.9 antigen in a mouse host.[9,15] Using ^{89}Zr-5B1 with and without preloading of unlabeled 5B1, we investigated the effect of preloading on ^{89}Zr-5B1 imaging in the context of circulating CA19.9. Our data suggest that the preloading of cold mAb improves the usefulness of ^{89}Zr-5B1 as an imaging agent to visualize disease in this mouse model, which may be applicable to current ongoing clinical trials with MVT-2163, the clinical grade preparation of ^{89}Zr-5B1.

EXPERIMENTAL SECTION

CA19.9 ELISA. The CA19.9 levels in serum samples from mice with subcutaneous Capan-2 xenografts were analyzed using a commercially available solid-phase sequential ELISA kit (Sigma-Aldrich) per the manufacturer's instructions. Blood (~200 μL) was collected from treatment naïve mice via a retro-orbital bleed, stored at 4 °C for 24 h in Eppendorf tubes, and separated by centrifugation at 2000*g* for 12 min. Analysis was carried out on undiluted as well as samples that were diluted 3-fold and 10-fold in phosphate-buffered saline (PBS) in order to ensure the CA19.9 concentrations in the sample fell within the calibration curve. All serum samples were stored at −20 °C and thawed slowly on ice prior to analysis.

Preparation of ^{89}Zr-5B1. Human recombinant 5B1 antibodies were purified from supernatant produced by a stable CHO-S production cell line grown in serum-free culture medium in a Wave bioreactor. Antibodies were purified by Protein A affinity chromatography (MabSelect, GE Healthcare) and buffer exchanged by dialysis into 10 mM phosphate, 150 mM NaCl, pH 6.0 buffer for storage at 4 °C. The purity was >95% (combined heavy and light chain) as estimated by SDS-PAGE under reducing conditions. 5B1 antibodies (3.0 mg, 4.6 mg/mL; lot 140827) in PBS buffer (pH 6.0) was adjusted to pH 8.5 using sodium bicarbonate solution (200 mM) and functionalized with *p*-isothiocyanatobenzyl-desferrioxamine (DFOBz-NCS; Macrocyclics, Inc.) with a 1:4 mAb/DFO-Bz-NCS ratio. In brief, a volume of 8.0 μL of DFO-Bz-NCS (13.3 mM in dimethyl sulfoxide) was added to 650 μL of 5B1, and the reaction was incubated at 37 °C for 1.5 h. The DFO modified antibodies were purified via a PD10 desalting column (GE Healthcare) into PBS pH 7.4. This intermediate was radiolabeled as previously described,[10] purified with a PD-10 gel-filtration column (GE Healthcare) into 0.9% saline solution, and used without further formulation. Radiochemical purity was assessed by instant thin layer chromatography (iTLC) on silica-impregnated paper strips that were read with an AR-2000 radioTLC plate reader (Bioscan Inc.) and analyzed with Winscan Radio-TLC software (Bioscan Inc.). ^{89}Zr was produced at Memorial Sloan Kettering Cancer Center (MSK) using an EBCO TR19/9 variable-beam energy cyclotron (Ebco Industries Inc.) by the ^{89}Y(p,n)^{89}Zr reaction.[16]

Cell Culture and Animal Models. All of the animal experiments were done in accordance with a protocol approved by the MSK Institutional Animal Care and Use Committee, and all xenografts studies were performed in 6−8 week old female, athymic nude mice, strain Crl:NU(NCr)-Foxn1^{nu}. Capan-2 cells were grown in Dulbecco's modified essential medium (DMEM) modified to contain 4.5 g/L glucose and supplemented with 20% (v/v) heat-inactivated fetal calf serum, 100 IU penicillin, and 100 μg/mL streptomycin. Subcutaneous Capan-2 xenografts were inoculated into the right flank using 5×10^6 cells suspended in 150 μL of a solution containing a 1:1 mixture of Matrigel (Corning) and cell culture medium. Capan-2 tumors were grown for 21−28 days postimplantation to an average tumor size of 200 mm^3 prior to imaging or biodistribution.

For orthotopic pancreas xenografts, athymic homozygous nude mice, strain Crl:NU(NCr)-Foxn1^{nu} (Charles River

DOI: 10.1021/acs.molpharmaceut.6b01130
Mol. Pharmaceutics 2017, 14, 908−915

Laboratories) age 6−8 weeks were used. Mice were anesthetized with 1−2% isoflurane gas in medical air at a rate of 2 L/min, and surgery was performed on a heated platform to help maintain body temperature. Bupivicaine, a local anesthetic agent, was injected intradermally in the area surrounding the incision line. Skin was prepped for surgery using alternating scrubs of povidone-iodine and 70% ethanol. A longitudinal incision (0.5−1 cm in length) was made in the skin and the peritoneum, allowing for the spleen and pancreas to be exteriorized. Capan-2 cells (2×10^6 cells in 30 μL containing 1:1 cell media and Matrigel) were slowly injected into the parenchyma of the pancreas. The spleen and pancreas were returned to the peritoneal cavity, the peritoneal wall was closed using 4−0 Vicryl sutures, and the skin was closed using sterile wound clips. Meloxicam was administered prior to recovery and dosage repeated postsurgery as needed every 4−24 h. Tumors reached optimal size within 14−21 days postimplantation.

Biodistribution. Biodistribution studies were designed to first determine the effect of the amount of time between injection of the unlabeled 5B1 and ^{89}Zr-5B1. Then, further studies were performed to determine the effect of injecting different amounts of cold 5B1 at the optimal time point determined from the previous study. Finally, the uptake of the tracer from 24 to 120 h was followed, using the optimized approach.

Biodistribution studies were performed as previously reported.[8,10] In brief, mice (n = 4−5 per time point) were injected via the lateral tail vein with ^{89}Zr-5B1(~30 μg, 135 ± 3 μCi) between 5 min and 24 h after the injection of unlabeled 5B1 (40−250 μg) also via tail vein or without administration of 5B1. Tissues of interest, including tumors in the subcutaneous xenograft model, were harvested between 24 and 120 h postinjection. The weight of each tissue sample was determined, and the localization of the tracer was analyzed by gamma counting and calibrating to standards of known activity. All activity concentrations from the biodistribution studies are expressed as the percentage of the injected dose per gram of tissue.

PET and PET/CT Imaging. A subset of mice (n = 3) used in the biodistribution studies were selected for PET imaging experiments, which were performed as previously described.[8,10] Imaging studies in mice with subcutaneous xenografts were performed with a microPET Focus scanner (Concorde Microsystems), whereas PET/CT imaging of mice with orthotopic xenografts was performed on an Inveon PET/CT scanner (Siemens Healthcare Global) between 4 and 120 h postinjection of the radiotracer. All of the resulting images were analyzed using ASIPro VM software. Further details are provided in the Supporting Information.

Statistical Analysis. All biodistribution and tumor to tissue ratio are reported as the average value ± SD. Statistical analysis was performed using a two-tailed Student's t test with $p < 0.05$ being considered significant.

RESULTS

Serum samples isolated from mice bearing subcutaneous Capan-2 xenografts of mass ranging from 75 to 1400 mg were analyzed to quantify the circulating CA19.9 levels. We observed a correlation between the tumor size and CA19.9 serum levels, although serum CA19.9 levels were more variable in tumors with masses of >500 mg (Figure 2A). When divided into four subgroups based on tumors size, <250 mg, 250−500 mg, 500−750 mg, and >750 mg, the CA19.9 serum levels were

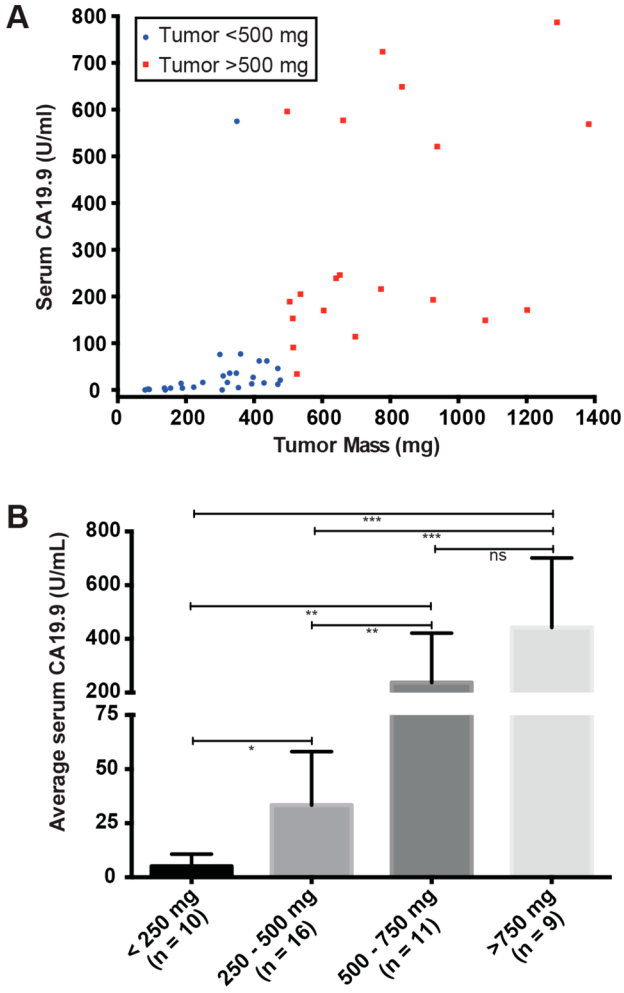

Figure 2. Serum levels of CA19.9 in mice with Capan-2 xenografts were analyzed by ELISA indicating that larger tumor sizes lead to increased CA19.9 (A) and that there was a statistically significant difference (* = $p < 0.05$; ** = $p < 0.001$; *** = $p < 0.0001$) across tumors of varying size (B).

significantly different between every set of groups with the exception of the 500−750 mg and >750 mg groups (Figure 2B). We chose to use animals bearing tumors between the sizes 150 to 400 mg for imaging and biodistribution in order to provide a consistent and relevant model for our investigations.

DFO-5B1 was radiolabeled with good specific activity (4.6 mCi/mg) and radiochemical purity (>98%), providing material for the imaging and biodistribution studies. To ensure comparability of results, approximately the same amount, both in terms of mass and activity, were injected for all experiments. Serial imaging experiments were performed in mice with subcutaneous Capan-2 xenografts without injection of 5B1 prior to ^{89}Zr-5B1 to provide a point of comparison for subsequent experiments employing the preloading strategy. The level of radiotracer in tumor tissue was apparent in tomographic slices of each of the mice that were imaged, and biodistribution was performed at 120 h in the same cohort of mice confirmed good tracer uptake (25.8 ± 4.4%ID/g). The maximum intensity projections (MIPs) (Figures 3A and S1) showed that the highest activity concentration in all the mice that were imaged was in the ipsilateral lymph nodes as early as 4 h postinjection, and the biodistribution showed high levels in

DOI: 10.1021/acs.molpharmaceut.6b01130
Mol. Pharmaceutics 2017, 14, 908−915

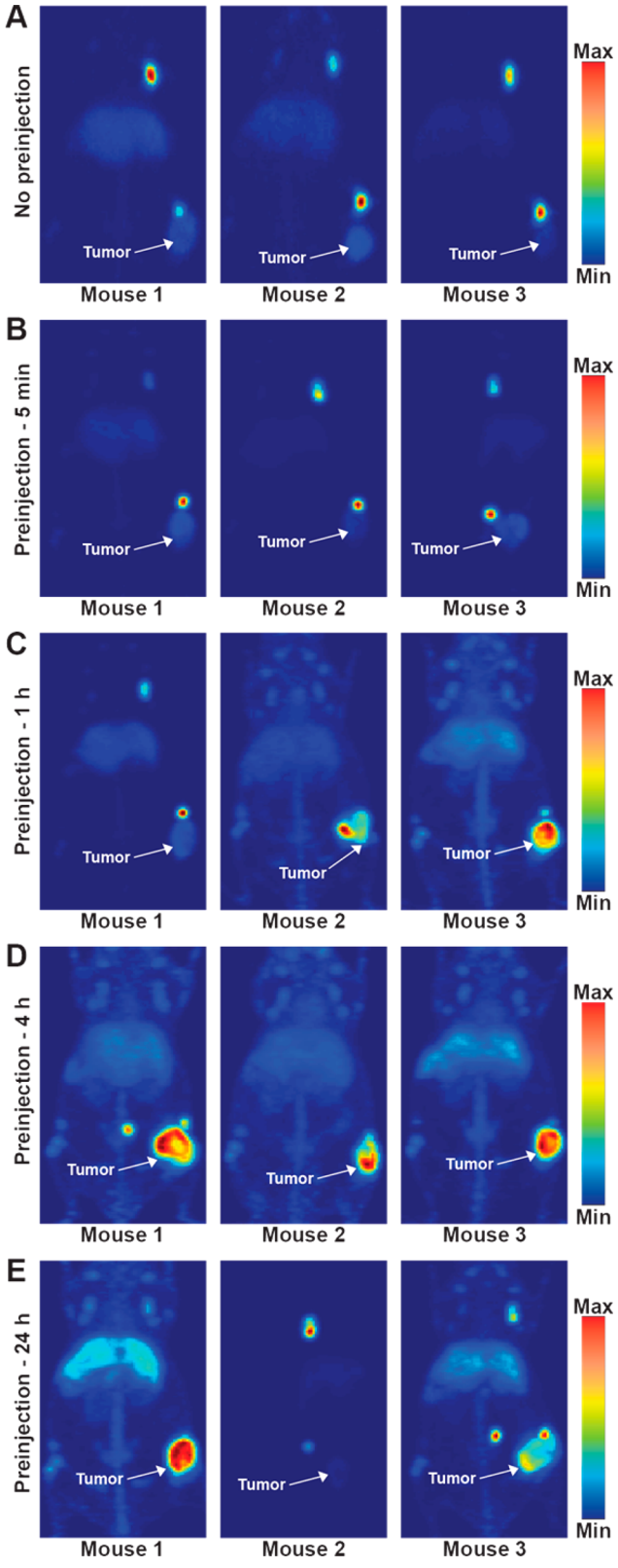

Figure 3. Maximum intensity projections of mice that were injected with ^{89}Zr-5B1 without preloading (A) or with preloading of 100 μg of unlabeled 5B1 at 5 min (B), 1 h (C), 4 h (D), or 24 h (E) prior to injection of ^{89}Zr-5B1.

liver and spleen, leading to low tumor to liver and tumor to spleen ratios.

To evaluate the effect of varying the time between injection of the 5B1 and administration of ^{89}Zr-5B1, a high dose (100 μg) of cold 5B1 was injected 5 min, 1, 4, or 24 h prior to injection of ^{89}Zr-5B1. Imaging (Figures 3 and S2) and biodistribution (Figure 4 and Table S1) at 120 h postinjection

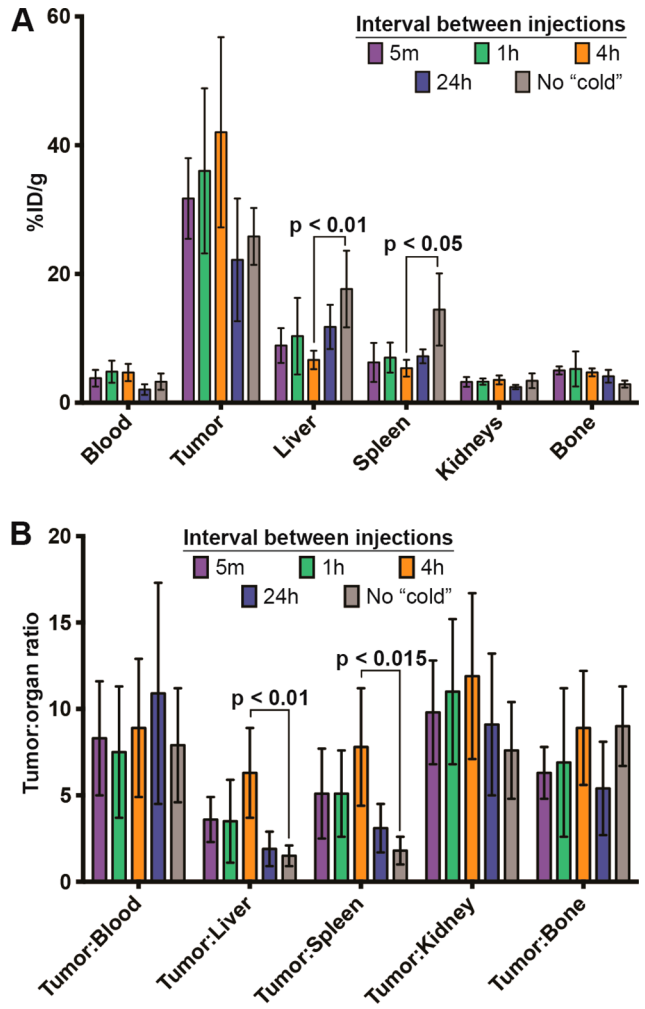

Figure 4. Bar graphs depicting activity concentration (A) and tumor to tissue ratios (B) in selected tissues as determined by biodistribution studies at 120 h postinjection of ^{89}Zr-5B1.

allowed for comparison of the various preloading schedules relative to no preloading of cold antibody. In mice injected with 5B1 5 min prior to ^{89}Zr-5B1, there was little to no perceptible difference relative to the cohort not administered 5B1. However, biodistribution studies showed a marginal improvement in tumor uptake and in the tumor-to-liver and tumor-to-spleen ratios.

A more pronounced improvement in image quality, relative to ^{89}Zr-5B1 alone, was observed in mice that were preloaded 1 h before ^{89}Zr-5B1, although the results were variable between mice. The MIPs for mouse 2 and 3 from the 1 h cohort showed uptake of radiotracer primarily in the tumor tissue, whereas uptake in mouse 1 was highest in the ipsilateral lymph nodes (Figure 3C). Biodistribution data shows that the uptake and tumor to tissue ratios were improved relative to no preloading of cold 5B1, but they were essentially identical to the 5 min cohort. The most pronounced improvement in terms of image

DOI: 10.1021/acs.molpharmaceut.6b01130
Mol. Pharmaceutics 2017, 14, 908−915

Table 1. Biodistribution of ^{89}Zr-5B1 in Mice Harboring Subcutaneous Capan-2 Xenografts That Were Injected with Cold 5B1 4 h Prior to Injection of the Indicated Amount of Radiotracer; All Values Are Reported as %ID/g

	100 μg preloading				40 μg preloading	250 μg preloading
organ	24 h	48 h	72 h	120 h	120 h	120 h
blood	12.5 ± 1.5	11.0 ± 2.2	7.3 ± 1.8	4.5 ± 2.2	4.7 ± 1.5	5.6 ± 1.3
tumor	23.4 ± 4.6	35.6 ± 6.6	28.7 ± 9.9	44.0 ± 12.3	44.1 ± 11.5	54.7 ± 25.3
heart	3.5 ± 0.8	3.2 ± 0.5	2.1 ± 0.1	1.5 ± 0.6	1.7 ± 0.5	1.8 ± 0.3
lungs	7.2 ± 2.4	5.3 ± 1.3	3.4 ± 0.8	2.6 ± 1.0	3.0 ± 0.8	4.2 ± 1.2
liver	6.8 ± 1.2	8.6 ± 2.2	9.5 ± 4.1	14.3 ± 5.8	16.1 ± 6.7	13.2 ± 3.1
spleen	5.0 ± 1.6	5.4 ± 1.5	3.8 ± 0.7	7.9 ± 2.9	11.6 ± 7.7	7.6 ± 0.5
pancreas	1.0 ± 0.1	1.0 ± 0.1	0.8 ± 0.1	0.6 ± 0.2	0.7 ± 0.1	0.8 ± 0.1
stomach	0.6 ± 0.1	0.8 ± 0.2	0.7 ± 0.2	0.4 ± 0.2	0.7 ± 0.2	0.7 ± 0.1
small intestine	1.1 ± 0.1	1.0 ± 0.3	0.9 ± 0.3	0.6 ± 0.3	0.7 ± 0.1	0.8 ± 0.2
large intestine	0.7 ± 0.1	0.7 ± 0.1	0.8 ± 0.2	0.5 ± 0.1	0.6 ± 0.1	0.7 ± 0.2
kidneys	6.8 ± 3.6	5.1 ± 0.4	4.8 ± 1.0	4.1 ± 1.0	4.2 ± 0.3	4.7 ± 0.7
muscle	0.9 ± 0.1	0.8 ± 0.2	0.7 ± 0.1	0.4 ± 0.2	0.6 ± 0.2	0.6 ± 0.1
bone	3.8 ± 0.7	5.1 ± 0.9	4.7 ± 1.9	6.6 ± 0.6	7.1 ± 0.3	8.2 ± 0.9

quality, tumor-to-liver ratio, and tumor-to-spleen ratio was achieved by preloading 4 h before the radiotracer (Figure 3D).

In this case, both the tumor-to-liver and tumor-to-spleen ratios were significantly different than those obtained with no preloading ($p < 0.01$ and $p < 0.05$, respectively) (Figure 4 and Table S1). Additionally, each of the images acquired showed the highest activity concentration in the tumor tissue, rather than the lymph nodes.

Image quality after waiting 24 h between the injection of 5B1 and ^{89}Zr-5B1 was not as robust as the 4 h preloading cohort. Marginal improvement in image quality (Figure 3E) and contrast was achieved, but the improvement is belied by the essentially identical tumor uptake (22.2 ± 9.6%ID/g) relative to the no preloading cohort (25.8 ± 4.4%ID/g) and significantly lower uptake relative to the 4 h cohort (42.2 ± 14.9%ID/g). Waiting for 24 h to administer ^{89}Zr-5B1 also results in lower tumor-to-liver and tumor-to-spleen ratios (Figure 4 and Table S1).

A biodistribution study was performed in mice with subcutaneous Capan-2 xenografts to assess the level of ^{89}Zr-5B1 over time, between 24 and 120 h, in mice that received 100 μg of 5B1 4 h prior to the radiotracer (Table 1). Using this optimized time point, we observed rapid uptake of radiotracer in the tumor tissue and a concomitant decrease of the activity concentration in the blood over time. High tumor-to-tissue contrast was achieved.

To study the effect of changing the dose level of cold antibody injected, 40, 100, or 250 μg of 5B1 was injected 4 h prior to ^{89}Zr-5B1, and the uptake at 120 h postinjection was assessed by biodistribution (Tables 1 and S2). Injection of 40 μg had similar effect on the distribution of ^{89}Zr-5B1 compared to 100 μg, showing essentially identical average tumor uptake and marginally higher uptake in the liver and spleen. Similarly, increasing the amount of 5B1 to 250 μg appeared to have similar overall distribution of ^{89}Zr-5B1. The uptake values for all three cohorts showed no statistically significant difference in the uptake or tumor to tissue ratio in any organ at 120 h postinjection of ^{89}Zr-5B1.

In order to assess this system in a model that simulates human disease dissemination, PET and PET/CT studies using the optimized parameters (preloading with 100 μg of unlabeled 5B1 4 h prior to tracer administration) were performed in mice bearing tumors orthotopically implanted into the body of the pancreas. PET images showed rapid uptake in the tumor at 48 h and improved contrast at 120 h postinjection (Figure 3A). PET/CT images acquired 120 h postinjection of ^{89}Zr-5B1 provided anatomical reference (Figure 3B). Images of both mice show differing levels in the inguinal, axillary, and mesenteric lymph nodes, the latter having the highest activity concentration of the three.

DISCUSSION

^{89}Zr-5B1 recently entered clinical trials as the investigational agent MVT-2163 for use as a staging and diagnostic tool for CA19.9 positive metastatic pancreatic cancer. Since CA19.9 can be found both as a soluble form circulating in the blood and as a highly expressed tumor surface antigen, there is the potential for improved images with preloading of unlabeled of 5B1, known as MVT-5873 clinically, to bind circulating CA19.9. We sought to determine the best approach for image enhancement using preclinical models of pancreatic cancer that are known to shed CA19.9 into circulation.

For evaluation of the preloading method, we selected the Capan-2 xenograft model, a human pancreatic cancer cell line that has been reported to shed CA19.9 into the circulation.[9,15] We evaluated the serum concentrations of CA19.9 from treatment naïve tumor bearing mice and found mouse serum levels to be proportional to tumor size. CA19.9 levels ranged from almost undetectable in animals with small tumors to approximately 800 U/mL in mice with large tumors. These levels correlate roughly to human levels that are low to moderate, with 0−37 U/mL being considered normal in healthy individuals. We chose to use mice with tumor volumes averaging 200 mm^3 because they generally shed a consistent and moderate level of CA19.9.

We established a baseline uptake of ^{89}Zr-5B1 in our model via imaging experiments and terminal biodistribution in which no preloading of cold tracer was administered. This approach yielded images of reasonable quality, but the tumor-to-tissue uptake ratios in the liver and spleen were poor (1.5 ± 0.6 and 1.8 ± 0.8, respectively). Furthermore, mice with no preloading had the highest activity concentrations in the ipsilateral inguinal and axillary lymph nodes, which are prominent in the MIPs (Figure 3A). The uptake in the nodes was rapid, with high activity concentrations seen at 4 h postinjection (Figure S1), the earliest imaging time point. This is not unexpected for such systems as those organs are the primary route of clearance for antibodies and shed antigens. In humans, the mesenteric lymph

DOI: 10.1021/acs.molpharmaceut.6b01130
Mol. Pharmaceutics 2017, 14, 908−915

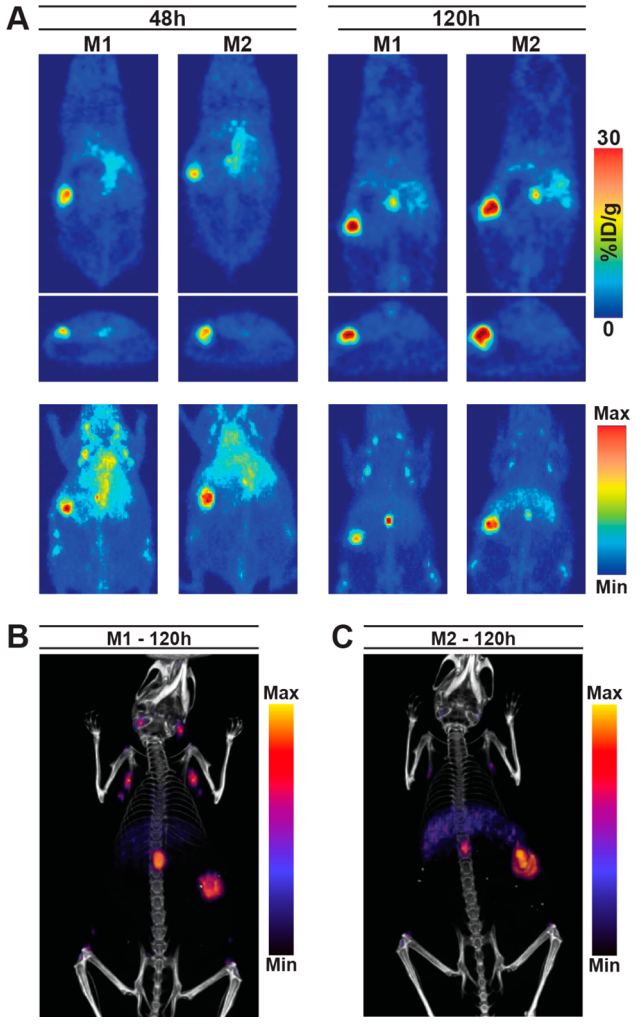

Figure 5. PET imaging studies in two mice with orthotopically implanted capan-2 xenografts that were administered 100 μg of unlabeled 5B1 4 h prior to ^{89}Zr-5B1. Tomographic slices and MIPs from PET scans at 48 and 120 h postinjection (A) as well as PET/CT images (B,C) acquired at 120 h postinjection of ^{89}Zr-5B1 are shown.

nodes are located proximal to the pancreas and the mesenteric artery, and interaction or encapsulation of the mesenteric artery determines a patient's candidacy for surgical resection in nonmetastatic pancreatic cancer; therefore, a high contrast image in this region would be helpful for accurate disease staging via PET in humans.

Admittedly, the interpretation of these results is complicated. It is known that CA19.9 is shed from Capan-2 cells, and we have previously shown that 5B1 bound to CA19.9 on the surface of Capan-2 cells is rapidly internalized, leading to retention of the labeled 5B1 inside the cell and resultant tumor accumulation.[9] As such, it is not easy to determine the source of the tracer that is localized to the lymph nodes, and indeed, there are several possible explanations. One possibility is that the tracer binds to circulating antigen and is sequestered in the lymph nodes. Another possibility is that the tracer binds at the tumor site where it is subsequently internalized and released into the lymphatic system. A third possibility is that Capan-2 cells, which are derived from a primary tumor having a low metastatic score,[17,18] have metastasized to the lymph nodes and the tracer is accumulating in tumor tissue. Given the low metastatic potential, the short incubation time of the xenografts, and the lack of any reports of subcutaneous Capan-2 xenografts metastasizing, the first two options seem much more plausible than the third, especially considering that accumulation in tumor tissue is increased by preloading, whereas localization to lymph nodes is drastically reduced. It is entirely possible that the tracer localized in the lymph nodes results from a combination of both processes. However, our knowledge of pancreatic lymph node drainage and associated pancreatic tumor metastases is limited, and this phenomena in the model at hand remains open to interpretation.[19]

Previous studies with ^{89}Zr-rituximab indicated that the preloading could potentially cause blocking of the antigen in the tumor, reducing uptake of the radiotracer, suggesting that the amount of mass of unlabeled antibody relative to the size of the antigen sink would be a consideration for this approach.[12] Also, the results of the trials with ^{89}Zr-rituximab and ^{89}Zr-trastuzumab suggest that the timing of the preloading might influence image quality. Thus, we evaluated the impact of these two primary factors on the improvement of PET tracer uptake and PET image contrast for ^{89}Zr-5B1 by studying the optimal timing between an injection of unlabeled 5B1 and ^{89}Zr-5B1, as well as the amount of unlabeled 5B1 that was injected prior to the imaging agent.

The 5 min preloading time point was chosen to mimic coadministration of cold and labeled antibody similar to ^{89}Zr-trastuzumab administration in humans. While this approach gave slightly improved tumor to liver and spleen ratios, the tumor uptake and contrast in the images was not significantly changed (Figure 3B). A potential explanation for this observation is that the unlabeled 5B1 had insufficient time to distribute and bind the CA19.9 in circulation.

The time course described here suggests that waiting 4 h between injections will give the best results in terms of image quality and tumor to tissue activity concentration ratios. MIPs showed that the activity concentration was highest in the tumor in the 4 h cohort. In addition, the tumor to liver and spleen ratios were both higher than any other time point. This result has precedence as a 1−3 h lag between unlabeled rituximab and ^{89}Zr-rituximab showed improved tumor contrast.[12] Given the improvement seen by preloading at 4 h, we sought to determine if allowing more time between injections would provide further improvement.

However, allowing 24 h between the 5B1 and ^{89}Zr-5B1 injections resulted in only marginally improved image quality and resulted in similar or even lower uptake relative to no preloading dose. Also, the tumor to liver and spleen ratios are much lower than with a 4 h preloading, suggesting that unlabeled compound may have bound in the tumor, blocking the subsequent binding of ^{89}Zr-5B1.

With an optimal preloading time point established, we also investigated the effect of changing the amount of unlabeled 5B1 that was preloaded 4 h prior to injection of ^{89}Zr-5B1. Lowering the mass of unlabeled 5B1 to 40 μg had essentially no effect on the activity concentrations in the tumor and other tissues (Table 1). The same was true of increasing the mass to 250 μg of 5B1. This suggests that all doses saturate the CA19.9 in circulation, and the minimal loading dose required to see improved image quality in this model was not determined. Finally, we evaluated a 100 μg preloading dose 4 h prior to injection of ^{89}Zr-5B1 in a Capan-2 orthotopic xenograft model in which the tumors were implanted directly into the body of the pancreas (Figure 5). PET and PET/CT images showed that we are able to delineate the tumor tissue in the pancreas and

DOI: 10.1021/acs.molpharmaceut.6b01130
Mol. Pharmaceutics 2017, 14, 908−915

that there is little nonspecific uptake in healthy tissues. While these results are also promising, this is still not an ideal preclinical model for evaluating CA19.9 radiotracers because mice do not endogenously express CA19.9. Regardless, we believe these results may justify the use of a preloading strategy if and when circulating antigen reduces image quality in patients.

In summary, these studies represent a systematic evaluation of a preloading strategy for antibody based PET imaging in a system with shed, circulating antigen. We demonstrate that adopting a preloading strategy can improve tumor uptake, increase tumor-to-tissue ratios, and reduce background uptake in nontarget organs in both subcutaneous and orthotopic mouse models of pancreatic cancer. These data may inform a strategy that could prove beneficial in clinical trials of ^{89}Zr-5B1, as well as future 5B1-based RIT, which is currently under investigation.

■ ASSOCIATED CONTENT

Supporting Information

The Supporting Information is available free of charge on the ACS Publications website at DOI: 10.1021/acs.molpharmaceut.6b01130.

All images acquired for each mouse in this study as well as all activity concentration and uptake ratios are reported (PDF)

■ AUTHOR INFORMATION

Corresponding Author

*E-mail: lewisj2@mskcc.org. Phone: 646-888-3038.

ORCID

Jacob L. Houghton: 0000-0003-4255-3044

Present Address

[&]Department of Radiology and Radiological Sciences, Vanderbilt University Medical Center, Nashville, Tennessee 37232, United States.

Notes

The authors declare the following competing financial interest(s): Wolfgang Scholz is an employee of Mabvax Therapeutics.

■ ACKNOWLEDGMENTS

We would like to thank the staff of the MSKCC Small Animal Imaging Core Facility as well as the Radiochemistry and Molecular Imaging Probe core. The authors also acknowledge the generous support of The Mr. William H. and Mrs. Alice Goodwin and the Commonwealth Foundation for Cancer Research as well as The Center for Experimental Therapeutics of Memorial Sloan Kettering Cancer Center. This work was supported in part by the NIH (1F32CA180452−01A1 and 5R25CA096945−09, to J.L.H.; 2R42CA128362 and HHSN261201300060C, to W.S.). The MSKCC Small Animal Imaging Core Facility as well as the Radiochemistry and Molecular Imaging Probe core were supported in part by NIH grant P30CA08748.

■ ABBREVIATIONS

PDAC, pancreatic ductal adenocarcinoma; CA19.9, carbohydrate antigen 19.9; PET, positron emission tomography

■ REFERENCES

(1) Rahib, L.; Smith, B. D.; Aizenberg, R.; Rosenzweig, A. B.; Fleshman, J. M.; Matrisian, L. M. Projecting cancer incidence and deaths to 2030: the unexpected burden of thyroid, liver, and pancreas cancers in the United States. *Cancer Res.* **2014**, *74* (11), 2913−21.

(2) Siegel, R.; Ma, J.; Zou, Z.; Jemal, A. Cancer statistics, 2014. *CA-Cancer J. Clin.* **2014**, *64* (1), 9−29.

(3) Rahib, L.; Fleshman, J. M.; Matrisian, L. M.; Berlin, J. D. Evaluation of Pancreatic Cancer Clinical Trials and Benchmarks for Clinically Meaningful Future Trials: A Systematic Review. *JAMA oncology* **2016**, *2*, 1209.

(4) Ballehaninna, U. K.; Chamberlain, R. S. The clinical utility of serum CA 19−9 in the diagnosis, prognosis and management of pancreatic adenocarcinoma: An evidence based appraisal. *Journal of gastrointestinal oncology* **2012**, *3* (2), 105−19.

(5) Rochefort, M. M.; Girgis, M. D.; Knowles, S. M.; Ankeny, J. S.; Salazar, F.; Wu, A. M.; Tomlinson, J. S. A mutated anti-CA19−9 scFv-Fc for positron emission tomography of human pancreatic cancer xenografts. *Molecular imaging and biology: MIB: the official publication of the Academy of Molecular Imaging* **2014**, *16* (5), 721−9.

(6) Girgis, M. D.; Olafsen, T.; Kenanova, V.; McCabe, K. E.; Wu, A. M.; Tomlinson, J. S. CA19−9 as a Potential Target for Radiolabeled Antibody-Based Positron Emission Tomography of Pancreas Cancer. *Int. J. Mol. Imaging* **2011**, *2011*, 834515.

(7) Girgis, M. D.; Kenanova, V.; Olafsen, T.; McCabe, K. E.; Wu, A. M.; Tomlinson, J. S. Anti-CA19−9 diabody as a PET imaging probe for pancreas cancer. *J. Surg. Res.* **2011**, *170* (2), 169−78.

(8) Houghton, J. L.; Zeglis, B. M.; Abdel-Atti, D.; Aggeler, R.; Sawada, R.; Agnew, B. J.; Scholz, W. W.; Lewis, J. S. Site-specifically labeled CA19.9-targeted immunoconjugates for the PET, NIRF, and multimodal PET/NIRF imaging of pancreatic cancer. *Proc. Natl. Acad. Sci. U. S. A.* **2015**, *112* (52), 15850−5.

(9) Houghton, J. L.; Zeglis, B. M.; Abdel-Atti, D.; Sawada, R.; Scholz, W. W.; Lewis, J. S. Pretargeted Immuno-PET of Pancreatic Cancer: Overcoming Circulating Antigen and Internalized Antibody to Reduce Radiation Doses. *J. Nucl. Med.* **2016**, *57* (3), 453−9.

(10) Viola-Villegas, N. T.; Rice, S. L.; Carlin, S.; Wu, X.; Evans, M. J.; Sevak, K. K.; Drobjnak, M.; Ragupathi, G.; Sawada, R.; Scholz, W. W.; Livingston, P. O.; Lewis, J. S. Applying PET to broaden the diagnostic utility of the clinically validated CA19.9 serum biomarker for oncology. *J. Nucl. Med.* **2013**, *54* (11), 1876−82.

(11) Sawada, R.; Sun, S. M.; Wu, X.; Hong, F.; Ragupathi, G.; Livingston, P. O.; Scholz, W. W. Human monoclonal antibodies to sialyl-Lewis (CA19.9) with potent CDC, ADCC, and antitumor activity. *Clin. Cancer Res.* **2011**, *17* (5), 1024−32.

(12) Muylle, K.; Flamen, P.; Vugts, D. J.; Guiot, T.; Ghanem, G.; Meuleman, N.; Bourgeois, P.; Vanderlinden, B.; van Dongen, G. A.; Everaert, H.; Vaes, M.; Bron, D. Tumour targeting and radiation dose of radioimmunotherapy with (90)Y-rituximab in CD20+ B-cell lymphoma as predicted by (89)Zr-rituximab immuno-PET: impact of preloading with unlabelled rituximab. *Eur. J. Nucl. Med. Mol. Imaging* **2015**, *42* (8), 1304−14.

(13) Oude Munnink, T. H.; Dijkers, E. C.; Netters, S. J.; Lub-de Hooge, M. N.; Brouwers, A. H.; Haasjes, J. G.; Schroder, C. P.; de Vries, E. G. Trastuzumab pharmacokinetics influenced by extent human epidermal growth factor receptor 2-positive tumor load. *J. Clin. Oncol.* **2010**, *28* (21), e355−6 author reply e357..

(14) Jauw, Y. W.; Menke-van der Houven van Oordt, C. W.; Hoekstra, O. S.; Hendrikse, N. H.; Vugts, D. J.; Zijlstra, J. M.; Huisman, M. C.; van Dongen, G. A. Immuno-Positron Emission Tomography with Zirconium-89-Labeled Monoclonal Antibodies in Oncology: What Can We Learn from Initial Clinical Trials? *Front. Pharmacol.* **2016**, *7*, 131.

(15) Takamori, H.; Hiraoka, T.; Yamamoto, T. Expression of tumor-associated carbohydrate antigens correlates with hepatic metastasis of pancreatic cancer: clinical and experimental studies. *Hepato-gastroenterology* **1996**, *43* (9), 748−55.

DOI: 10.1021/acs.molpharmaceut.6b01130
Mol. Pharmaceutics 2017, 14, 908−915

(16) Holland, J. P.; Sheh, Y.; Lewis, J. S. Standardized methods for the production of high specific-activity zirconium-89. *Nucl. Med. Biol.* **2009**, *36* (7), 729−39.
(17) Kyriazis, A. A.; Kyriazis, A. P.; Sternberg, C. N.; Sloane, N. H.; Loveless, J. D. Morphological, biological, biochemical, and karyotypic characteristics of human pancreatic ductal adenocarcinoma Capan-2 in tissue culture and the nude mouse. *Cancer research* **1986**, *46* (11), 5810−5.
(18) Suemizu, H.; Monnai, M.; Ohnishi, Y.; Ito, M.; Tamaoki, N.; Nakamura, M. Identification of a key molecular regulator of liver metastasis in human pancreatic carcinoma using a novel quantitative model of metastasis in NOD/SCID/gammacnull (NOG) mice. *Int. J. Oncol.* **2007**, *31* (4), 741−51.
(19) Durczynski, A.; Hogendorf, P.; Szymanski, D.; Grzelak, P.; Strzelczyk, J. Sentinel lymph node mapping in tumors of the pancreatic body: preliminary report. *Wspolczesna Onkol.* **2012**, *16* (3), 206−9.

DOI: 10.1021/acs.molpharmaceut.6b01130
Mol. Pharmaceutics 2017, 14, 908−915